Chinese Chemical Letters 32 (2021) 1491–1496

Contents lists available at ScienceDirect

Chinese Chemical Letters

journal homepage: www.elsevier.com/locate/cclet

Communication

Highly N/O co-doped ultramicroporous carbons derived from nonporous metal-organic framework for high performance supercapacitors

Yangyi Gu, Ling Miao, Ying Yin, Mingxian Liu, Lihua Gan, Liangchun Li*

Shanghai Key Lab of Chemical Assessment and Sustainability, School of Chemical Science and Engineering, Tongji University, Shanghai 200092, China

ARTICLE INFO

Article history:
Received 10 August 2020
Received in revised form 15 September 2020
Accepted 16 September 2020
Available online 19 September 2020

Keywords:
N/O co-doped
Ultramicroporous
Metal-organic frameworks
Porous carbons
Supercapacitors

ABSTRACT

A new nonporous Zn-based metal-organic framework (NPMOF) synthesized from a high nitrogen-containing rigid ligand was converted into porous carbon materials by direct carbonization without adding additional carbon sources. A series of NPMOF-derived porous carbons with very high N/O contents (24.1% for NPMOF-700, 20.2% for NPMOF-800, 15.1% for NPMOF-900) were prepared by adjusting the pyrolysis temperatures. The NPMOF-800 fabricated electrode exhibits a high capacitance of 220 F/g and extremely large surface area normalized capacitance of 57.7 μF/cm^2 compared to other reported MOF-derived porous carbon electrodes, which could be attributed to the abundant ultramicroporosity and high N/O co-doping. More importantly, symmetric supercapacitor assembled with the MOF-derived carbon manifests prominent stability, *i.e.*, 99.1% capacitance retention after 10,000 cycles at 1.0 A/g. This simple preparation of MOF-derived porous carbon materials not only finds an application direction for a variety of porous or even nonporous MOFs, but also opens a way for the production of porous carbon materials for superior energy storage.

With the increasing demand for energy and power, it is urgent to find suitable energy storage equipments. As novel energy storage devices, supercapacitors have received more and more attention due to their higher power density, faster charge-discharge rate and longer cycle life than conventional batteries [1,2]. Supercapacitors can be divided into two types [3]. One is capacitors that undergo a Faraday electrochemical reaction at the electrode surface, also known as pseudocapacitors. The other is called electrochemical double-layer capacitors (EDLCs), which store energy by accumulating static charge in the electric double layer at the interface of the electrolyte and the electrode. EDLCs usually use porous carbons with high surface area as electrode materials.

The capacitance of supercapacitors mainly depends on the electrode materials. Carbon materials are the earliest electrode materials used in capacitors with large surface area, good electrical conductivity, thermal and chemical stability. They are also rich in resources and inexpensive [4,5]. For the future applications of porous carbon materials to supercapacitors, it mainly requires that porous carbon materials possess high surface area, reasonable pore size distribution, and high electrical conductivity and wettability [6–8]. In the field of energy storage, the high surface area is beneficial to increase the storage sites of carbon materials and the device energy density. But it is not general that the larger the surface area means the better performance. The matching of pore size and electrolyte ion size is also an important factor affecting the electrochemical properties [9,10]. Generally, porous carbons with uniform pore size distribution exhibit higher energy density. In addition, by introducing heteroatoms such as B, N, P and S, the wettability of materials can be improved and the pseudo-capacitive effect can also be introduced to enlarge the electro-chemical capacitance [11,12]. Porous carbon materials are readily prepared by pyrolysis of organic precursors (*e.g.*, polymers) and subsequent physical or chemical activation [13–16]. Albeit this method can produce porous carbon materials with high surface area, the pore size distribution is generally wide and the structure is highly disordered, impeding realization of the pore-electrolyte matching and further functionalization. In order to solve this problem, carbonization of crystalline metal-organic frameworks (MOFs) at various temperatures to produce relatively ordered porous carbons has been emerging as an effective strategy.

MOFs are crystalline materials constructed by self-assembly of organic ligands and metal ions (or clusters). As a new type of porous materials, due to their large surface area, adjustable pores

* Corresponding author.
E-mail address: lilc@tongji.edu.cn (L. Li).

https://doi.org/10.1016/j.cclet.2020.09.029

and active metal sites, MOFs show extraordinary potential in gas storage and separation, catalysis, ion exchange and electrochemistry [17–22]. MOFs have become the most attractive precursors and templates for the preparation of porous carbons due to their rich diversity and highly ordered porous structures [23,24]. Thus MOF-derived carbon materials often exhibit relatively controllable and narrow pore size distribution as well as good electrical conductivity and easy heteroatom-doping as active sites [6]. Xu *et al.* first introduced furyl alcohol (FA) into the pores of MOF-5 (Zn as the metal), and then carbonized in the argon atmosphere at 1000 °C to produce a porous carbon material with very high specific surface area (2872 m^2/g) and pore volume (2.06 m^3/g) [25]. Since then many other MOFs have been utilized in the field of electrochemistry as energy storage and conversion materials in virtue of their merits [26–32]. Among them, ZIFs rich in N heteroatoms of their organic ligands are frequently used to prepare electrode materials for supercapacitors [33–35]. Chaikittisilp *et al.* carbonized commercially available ZIF-8 without any other carbon sources, and the resultant porous carbons exhibited high electrochemical performance [36]. Except for the narrow pore size distribution and heteroatoms doping, ultramicroporosity of the porous carbons has been long-sought since it is propitious to efficient transportation of the small electrolyte ions and extremely high cycle stability, yet challenging in synthesis [9]. Direct carbonization of microporous or nonporous MOFs (NPMOFs) could be a promising and efficient way to prepare ultramicroporous carbons. In particular, numerous NPMOFs have hitherto been reported but much less investigated because of the useless nonporosity, and therefore exploration of their conversion to intriguing ultramicroporous carbons for high-performance electrodes are of great significant and worthy of intensive study.

In this context, an organic ligand with very high nitrogen content was successfully prepared and used to synthesize NPMOF. The NPMOF was directly carbonized under the temperature of 700 °C, 800 °C and 900 °C to obtain porous carbon materials, which were denoted as NPMOF-700, NPMOF-800 and NPMOF-900, respectively. Among them, the specific capacitance of the supercapacitor assembled by NPMOF-800 in 6 mol/L KOH is 220 F/g, which is very high compared with the reported MOF-derived carbon materials. Moreover, the two-electrode test showed that high capacitance and superb cycle stability could be achieved by NPMOF-800 electrode. The capacitance retention rate was over 99.1% after 10,000 charge-discharge cycles. These prominent performances were attributed to the intriguing structure of the NPMOF-derived porous carbons, *i.e.*, high nitrogen/oxygen doping, generated ultramicroporosity and narrow pore size distribution.

As demonstrated in the Fig. 1, firstly the high nitrogen-containing ligand (BITA, 37.82% N) was designed and readily synthesized in large scale (Supporting information). And then a straightforward solvothermal reaction of BITA with $Zn(NO_3)_2{\cdot}6H_2O$ afforded NPMOF as octahedron crystals (Fig. 1b). The crystal structure of NPMOF was intuitively characterized by single crystal X-ray diffraction and depicted in Figs. 1c, d and Fig. S1 (Supporting information), showing the nonporous nature with coordinated NO_3^- counter ions and MeCN molecules tightly encapsulated in the very small pores. Unlike the other highly porous MOFs the pores of which usually collapse or shrink during the high temperature carbonization, the easily decomposed NO_3^- ions and volatilized MeCN molecules in NPMOF should result in various gases such as H_2O and CO_2 released from the solid NPMOF crystals, facilitating the generation of ultramicropores. As a result, the MOF-derived porous carbon materials were readily prepared by pyrolysis at 700 °C, 800 °C and 900 °C, denoted as NPMOF-700, NPMOF-800 and NPMOF-900, respectively (Supporting information).

Scanning electron microscope (SEM) images confirm that the as-synthesized NPMOF consists of uneven dispersed crystals in

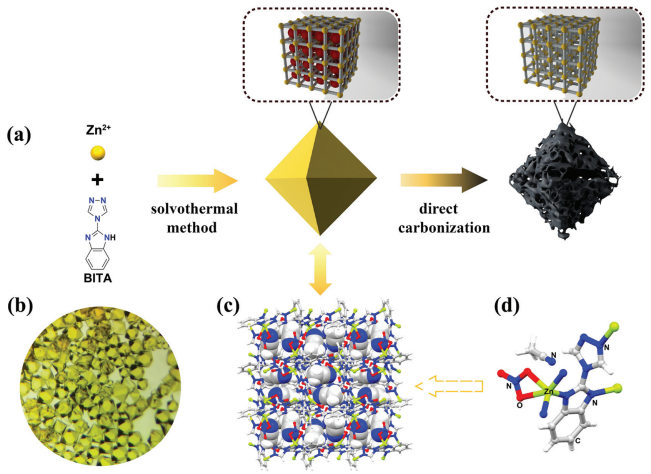

Fig. 1. Schematic illustration for the preparation of (a) MOF-derived porous carbonsand single crystal structure of NPMOF. (b) Photos of the NPMOF crystals. (c) Structure with encapsulated acetonitrile molecules showing in space-filling model. (d) The coordination state of Zn metal (gray: C atom, red: O atom, blue: N atom, yellow: Zn atom, white: H atom).

octahedron shape, and the diameters of NPMOF are ranged from 10 μm to 100 μm (Figs. 2a and b). As revealed by the SEM images, small-sized crystals of the obtained MOF-derived porous carbon materials largely retain the original octahedron shape from the parent NPMOF and exhibit a smooth surface without any large pores or cracks. In comparison, the large-sized particles splinter severely (Figs. 2c, d and Fig. S2 in Supporting information). The TEM images (Figs. 2e, f and Fig. S3 in Supporting information) intuitively show the nature of micropores, mesopores and macropores of the NPMOF-800 material.

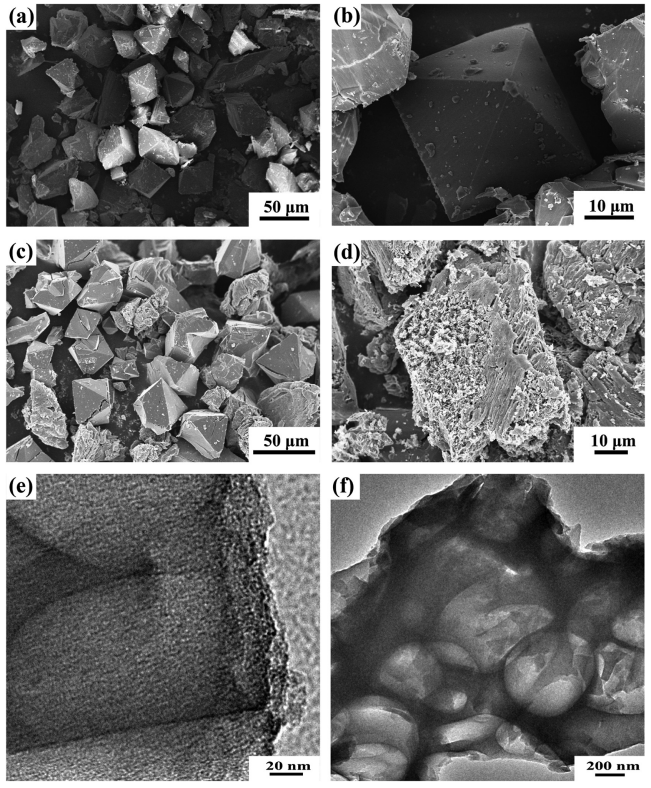

Fig. 2. SEM images of (a, b) NPMOF crystals and (c, d) NPMOF-800. (e, f) TEM images of NPMOF-800.

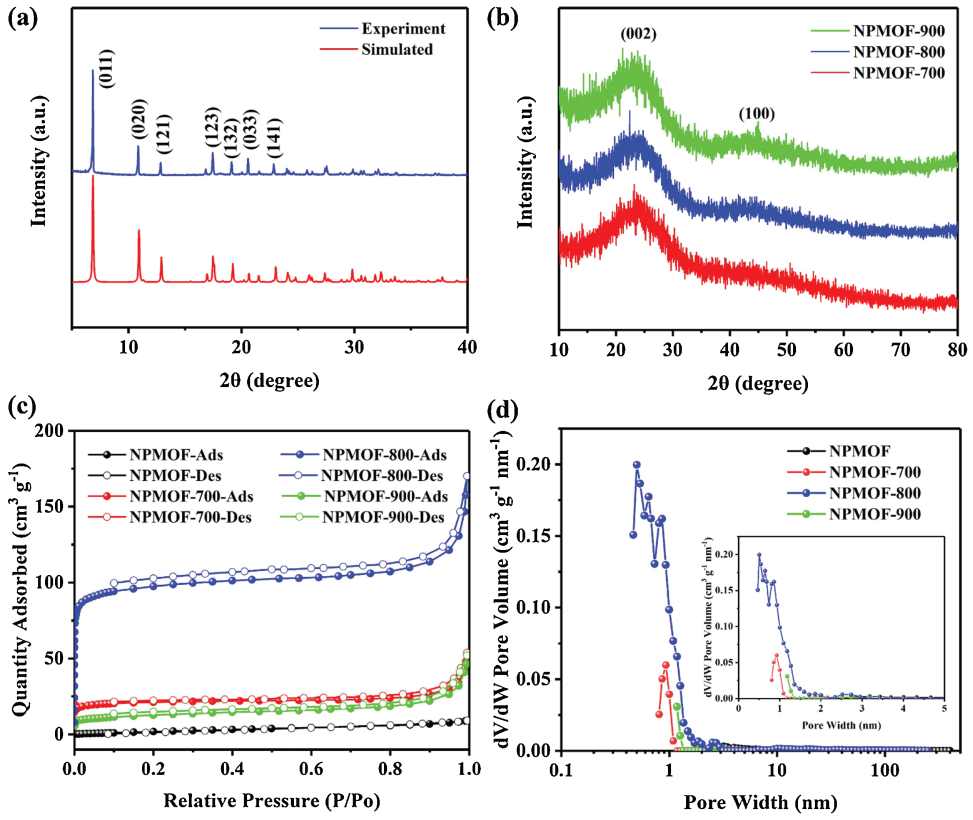

Fig. 3. XRD patterns of (a) NPMOF and (b) MOF-derived porous carbons. (c) Nitrogen sorption isotherms and (d) pore size distributions of NPMOF, NPMOF-700, NPMOF-800 and NPMOF-900.

The XRD patterns of the NPMOF are illustrated in Fig. 3a. The diffraction peaks of pristine NPMOF are in good agreement with the XRD patterns simulated from single crystal structure. After carbonization, the XRD patterns of the MOF-derived porous carbons exhibit broad diffraction peaks at 23° and 44° assignable to the typical (002) and (100) lattices of amorphous carbons (Fig. 3b) [37]. Thermogravimetric and differential scanning calorimetry (TG-DSC) curves of NPMOF were measured under nitrogen atmosphere, and gave a deep understanding for the carbonization process (Fig. S4 in Supporting information). The acetonitrile molecules begin to overflow at 60 °C. When the temperature reaches around 350 °C, the coordinated nitrates initiate the decomposition and the ligands start to degrade, giving out volatiles (*e.g.*, CO_2, H_2O) and facilitating the generation of ultramicropores [38]. Compared to the initial weight of NPMOF crystals, 60% weight loss is detected at 900 °C by TG analysis. The IR spectra of the MOF-derived porous carbons exhibit absorption peaks for C–N bending vibration (1290 cm^{-1}), and C=N stretching vibration in triazolidine rings (1450 cm^{-1}) (Fig. S5 in Supporting information).

Raman measurements were carried out to explore the detailed carbon structure. The Raman spectra for the MOF-derived porous carbons exhibit D and G bands located at 1350 cm^{-1} and 1580 cm^{-1}, respectively (Fig. S6 in Supporting information). These peaks are the components of the disordered carbon structure (D band) and graphitic carbon structure (G band) [39]. The relative ratios of D band to G band (I_D/I_G) are calculated based on the peak height to evaluate the crystallization degree of graphitic sp^2-type carbon (sp^2-C) structures [40]. The I_D/I_G value of NPMOF-900 (0.996) is the smallest and all the I_D/I_G values of NPMOF-derived porous carbons are *ca.* 1.0, indicating the high graphitization degree of these carbon materials.

The porosity of these MOF-derived carbons was investigated by N_2 sorption. The degassing process was conducted under vacuum conditions at 150 °C for 5 h before measurements. As shown in Fig. 3c, the NPMOF exhibits type I isotherms, and the MOF-derived porous carbons present the combined characteristics of type I and IV isotherms, along with a slightly upward tendency at $P/P_0 > 0.9$ [41]. The very low adsorption of NPMOF indicates its nonporous feature. The sharp N_2 uptakes at very low relative pressure ($P/P_0 < 0.1$) prove the presence of micropores [36]. In the range of 0.1 to 0.9 ($0.1 < P/P_0 < 0.9$), a little hysteresis loops are observed, attributed to the narrow slit-like pores. At high relative pressure ($P/P_0 > 0.9$), the N_2 uptakes are steep, indicating that the MOF-derived porous carbons may have some macropores embedded in the micropores (*e.g.*, interparticle voids) [36]. The nonlocal density functional theory (NLDFT) equilibrium model was applied to evaluate pore size distribution. As shown in Fig. 3d, the ultramicropores of the obtained MOF-derived porous carbons with diameters around 0.5 nm may be ascribed to the removal of Zn nanoparticles, and the micropores with diameters about 1 nm could be attributed to the volatilization of gases generated from the nitrates and pyrolysis of the BITA ligands.

Different carbonization temperatures led to a great impact on the porosity of the derived carbon materials. The Brunauer-Emmett-Teller (BET) surface areas (S_{BET}), micropore areas (S_{micro}), total pore volumes (V_{pore}) and micropore volumes (V_{micro}) of these porous carbons are summarized in Table S2 (Supporting information). The micropore volumes were calculated by the *t*-plot method. The NPMOF-800 possesses a relatively high surface area of 381 m^2/g, which is much higher than that of the NPMOF-700 (82 m^2/g). However, the surface area of the NPMOF-900 sample with higher graphitization dramatically decreased to 43 m^2/g. Furthermore, the ratio of the microporous volumes (V_{micro}/V_{pore}) in NPMOF-800 is almost three times of that in NPMOF-900,

contributing to the better electrochemical performance. Benefiting from the microporous structure, the surface areas of these MOF-derived porous carbons are very high compared with the parent NPMOF. The chemical and electronic states of the elements that exist within these porous carbons were further investigated *via* X-ray photoelectron spectroscopy (XPS). In the wide-scan XPS spectra (Fig. S7 in Supporting information), four peaks are observed and assigned to the typical peak of Zn 2p, C 1s, N 1s, O 1s at 1020.4 eV, 283.9 eV, 397.5 eV, 531.3 eV, respectively. As the temperature rises from 700 °C to 900 °C, the content of N decreases from 17.77% to 8.28%, and the content of C increases accordingly while the content of O is almost constant (Table S3 in Supporting information). The total N and O doping amount decreases from 24.08% for NPMOF-700 to 15.14% for NPMOF-900. It is notable that based on our strategy NPMOF-800 possesses highly graphitic structure, yet the N content still retains 13.91%.

The narrow-scan XPS spectra are presented in Fig. 4. The N 1s spectra of all the porous carbons can be mainly fitted into four peaks centered at ~ 397.4 eV, 398.8 eV, 399.9 eV and ~ 400.7 eV. The N_1 peak at 397.4 eV is assigned to the formation of Zn-N bonds (N atoms bonded to Zn atoms) [42]. The N_2 peak at 398.8 eV is corresponded to pyridinic-N (N-6) [41]. The N_3 peak centered at 399.9 eV is attributed to pyrrolic-N (N5) [43]. The N_4 peak at the highest binding energy (400.7 eV) undoubtedly represents graphitic-N (N-Q) [44]. It is revealed that various types of N atoms have been steadily doped into the carbon structure. N-6 and N-5 are considered to contribute to the faraday reaction and provide pseudocapacitance, while N-Q can increase the conductivity of the material. Moreover, the wettability of carbon materials can be further increased due to the different electronegativity of N and C atoms. The percentages of doped N content estimated from the XPS spectra are 17.77% (for NPMOF-700), 13.91% (for NPMOF-800) and 8.28% (for NPMOF-900). It is rational that the C—N bonds are gradually destroyed with the increasing of temperature, thereby leading to the lower N content in the NPMOF-900. The O 1s spectra are assigned to the following peaks: 530.6 eV is attributable to Zn-O [45], 531.6 eV is assignable to C=O and 532.7 eV is ascribed to C—O [46,47]. The C 1s spectra can be assigned into six peaks (Fig. S8 in Supporting information). The C_1 peak at ~283.0 eV is deconvoluted to metal carbide, while the C_2 peak at 284.0 eV is related to a graphitic carbon structure (sp^2-C) [48]. The C_3 peak at 284.8 eV belongs to sp^3 C—C [49]. The C_4 peak at 285.9 eV is assigned to C atoms directly bonded to oxygen (C—O) [48]. The C_5 peak at 286.2 eV is ascribed to sp^3 C—N [50]. The small peak centered around 287.6 eV (C_6) is related to C=O [48]. The binding energy values of Zn $2p_{3/2}$ and Zn $2p_{1/2}$ are found at 1022.0 eV and 1045.0 eV, respectively [42].

As energy storage and conversion devices, supercapacitors have both the characteristics of conventional capacitors and the batteries that can charge and discharge of capacitors rapidly and store energy. Recently the MOF-derived porous carbon materials have proved to show great potential in high-performance supercapacitors because of their unique structures and heteroatoms doping [51–53]. To evaluate the electrochemical properties of MOF-derived porous carbons, electrochemical experiments were carried out using a three-electrode system in 6 mol/L KOH electrolyte under the potential window of -1 V to 0 V. The CV and GCD curves of MOF-derived porous carbons electrodes conducted at different potential scan rates and current densities are shown in Fig. 5. The NPMOF-700 displays a distorted rectangular CV shape, whereas other electrodes present quasi-rectangular CV shapes (Fig. 5b). The distorted rectangular CV shape

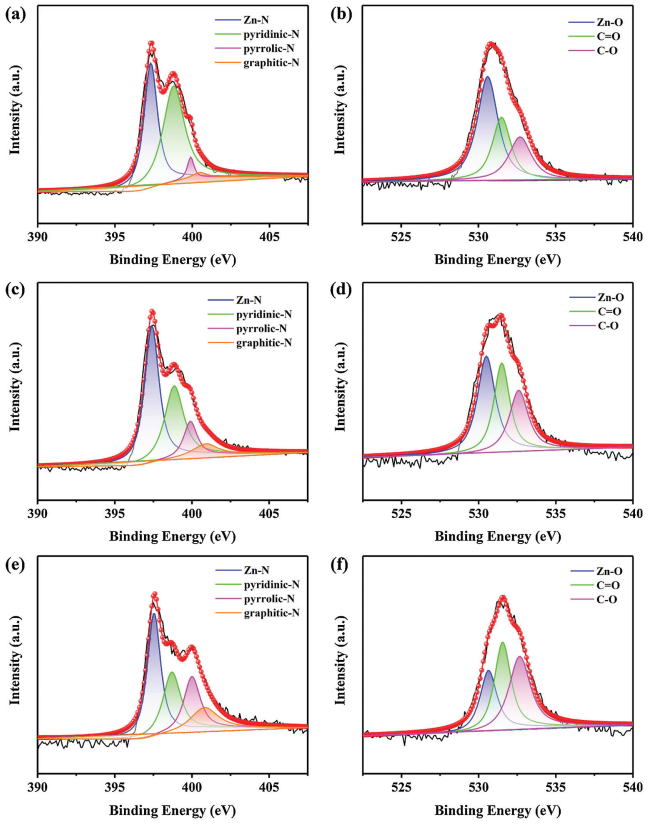

Fig. 4. High-resolution XPS spectra of NPMOF-700 ((a) N 1s, (b) O 1s), NPMOF-800 ((c) N 1s, (d) O 1s) and NPMOF-900 ((e) N 1s, (f) O 1s).

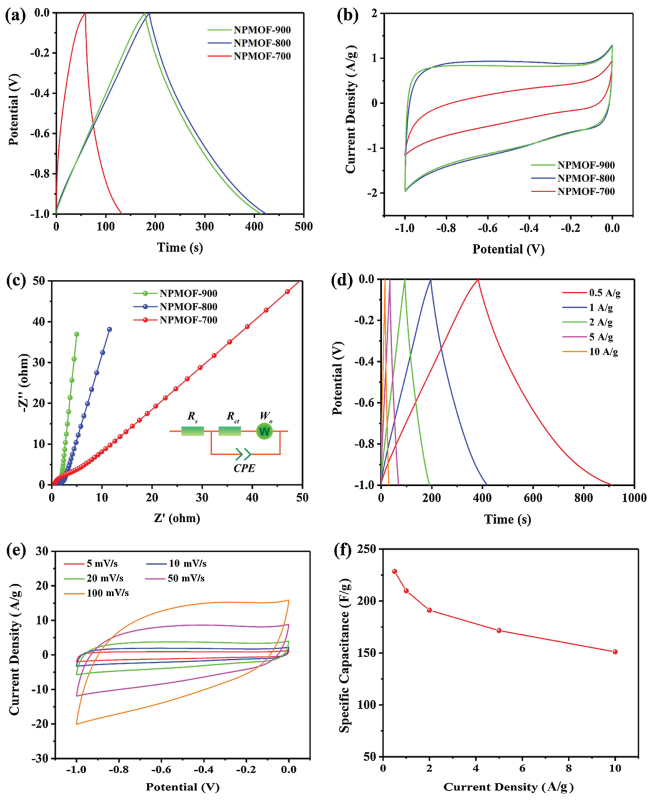

Fig. 5. Electrochemical performances measured in a three-electrode system using 6 mol/L KOH electrolyte: (a) GCD curves at 1 A/g. (b) CV curves at 5 mV/s. (c) Nyquist plotsof NPMOF-700, NPMOF-800 and NPMOF-900 electrodes. (d) GCD curves at different current densities. (e) CV curves at different scanning rates. (f) The relationships between current densities and capacitancesof NPMOF-800 electrodes.

indicates the ion-diffusion limitation in micropores [54]. The CV curves of NPMOF-800 electrode at varied scan rates from 5 mV/s to 100 mV/s retain relatively rectangular shapes, indicating good charge propagation with excellent rate capability (Fig. 5e). In order to evaluate the specific capacitance of the MOF-derived porous carbons electrodes, galvanostatic charge-discharge measurements were conducted at various current densities in a three-electrode system. All of the electrodes display a *quasi*-linear appearance with a slight bend, implying the pseudocapacitance impact derived from N/O doping. It is well known that the presence of some heteroatom (N, O, P, S, *etc.*) functionalities can enhance the capacitance by the pseudo-capacitive effect [55,56]. As shown in Fig. 5a, the specific capacitance values obtained at a current density of 1 A/g are 66 F/g (NPMOF-700), 220 F/g (NPMOF-800) and 207 F/g (NPMOF-900), respectively. These values are among the previously reported high capacitances of MOF-derived porous carbon electrodes (Table S4 in Supporting information) [31,36–58]]. Fig. 5a shows the charge-discharge curves at 1 A/g. NPMOF-800 is at a premium due to its larger surface area and pore volume. The specific capacitance of NPMOF-700 is only 66 F/g at a current density of 1 A/g, while it drastically increases to 220 F/g and 207 F/g for NPMOF-800 and NPMOF-900. Nyquist plots are applied to gain an insightful understanding of the ion-diffusion and charge-transfer behaviors within electrodes (Fig. 5c) [54]. For each sample, the Nyquist plot showed a small semicircle at high frequency and a linear trait at low frequency. At low frequencies, the vertical curve is featured, indicating a nearly ideal capacitive behaviour. The equivalent series resistance (R_s) calculated from the intercept point at the Z′-axis, are 0.50 Ω, 0.51 Ω and 0.53 Ω for NPMOF-700, NPMOF-800 and NPMOF-900 electrodes, respectively. The semicircle diameter represents the charge transfer resistance (R_{ct}), the fitted R_{ct} value of NPMOF-700 is 3.9 Ω, which was much higher than the value of NPMOF-800 (0.59 Ω) and NPMOF-900 (0.54 Ω), indicating lower speeds of electron transfer and ion transport. The charge transfer resistance is too high for NPMOF-700, which is the main reason leading to its poor performance. Additionally, the straight line of the Nyquist plot represents the warburg impedance (W). Clearly, the R_{ct} (0.59 Ω) and W (0.42 Ω) for NPMOF-800 can ensure the efficient electron transfer and fast ion diffusion.

In consideration of factors such as effective surface area, pore size distribution and heteroatom doping, NPMOF-800 delivers the most excellent electrochemical performance. It is worth mentioning that the BET surface area normalized capacitance of NPMOF-800 is 57.7 μF/cm^2 and among the highest values for all the porous carbon materials, which is ascribed to the abundant ultramicropores (Table S4 in Supporting information).

To further characterize the electrochemical performances of NPMOF-800 electrode, symmetric two-electrode devices were also assembled using 6 mol/L KOH electrolyte. The CV curves show a typical rectangular shape from 0 to 1 V with the sweep rates ranging from 5 mV/s to 100 mV/s, suggesting rapid electrochemical responses in aqueous electrolyte solutions (Fig. 6a) [40]. The CV shape is mirror-symmetric, even at a high scan rate, indicating the high reversibility of the sample. The charge-discharge current densities are varied from 0.2 A/g to 10 A/g to evaluate the specific energy and power of the device. All the GCD curves under various

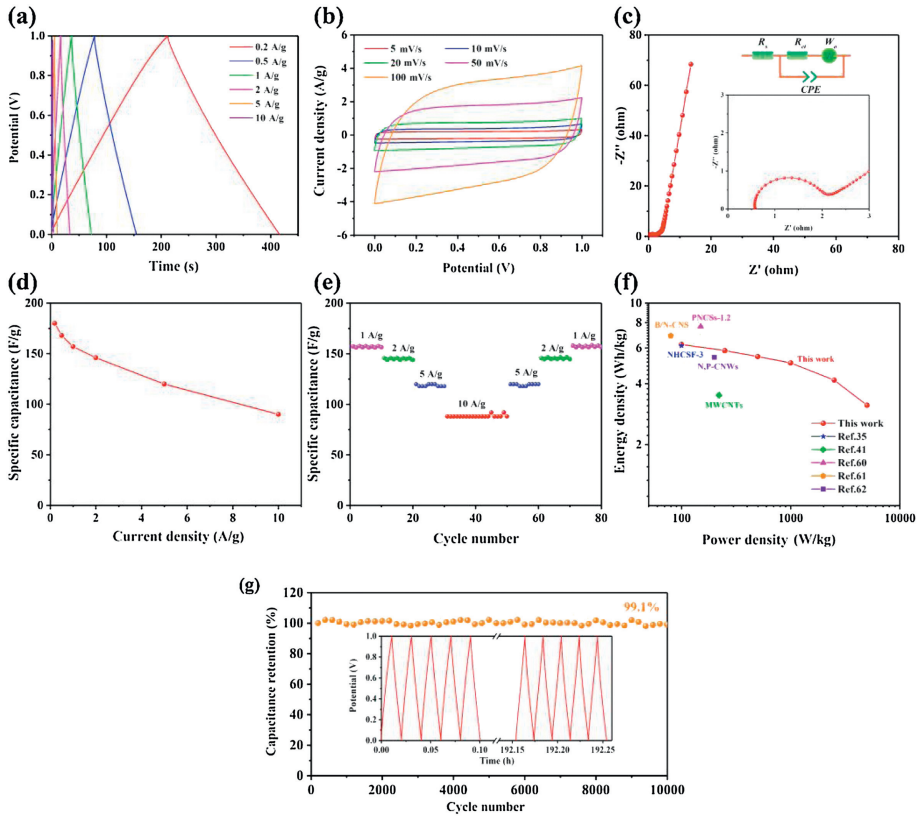

Fig. 6. Electrochemical performances of NPMOF-800 electrode measured in a two-electrode system using 6 mol/L KOH electrolyte: (a) GCD curves at different current densities. (b) CV curves at different scanning rates. (c) Nyquist plot. (d) The relationship between current densities and capacitances. (e) Rate performance measurements. (f) Ragone plot. (g) Cycling stability at 1 A/g.

current densities show typical linear discharge curves, demonstrating low internal resistances which are in consistent with EIS measurements [59]. Nyquist plots (Fig. 6c) demonstrate the positive effect of NPMOF-800 as a beneficial conductive scaffold due to the low R_s (0.41 Ω) and R_{ct} (1.3 Ω). The symmetric device shows a high capacitance value of 168 F/g (at 0.5 A/g). Ragone plot in relation to energy-power densities is displayed (Fig. 6f). At the current density of 0.2 A/g, the device exhibits high specific energy of 6.25 Wh/kg at the power of 100 W/kg. Furthermore, the specific energy maintains at 5.07 Wh/kg when the specific power increases to 1000 W/kg at 5 A/g. The energy density of NPMOF-800 device is comparable and even higher than other carbon materials reported previously [35,41,60–62]. To further demonstrate the advantages of NPMOF-800 for supercapacitors, the life cycle test was carried out using GCD studies at a current density of 1 A/g up to 10,000 cycles (Fig. 6g). After 10,000 cycles, NPMOF-800 device still remains over 99.1% of the initial specific capacitance, which is overwhelmingly high compared with previously reported values (Table S4). These results highlight the advantages of our symmetric capacitors meeting the requirements of high stability, excellent rate capability, and high cycle performance. These interesting features of this symmetric supercapacitor open a new era for researchers to explore high-performance electrochemical energy storage devices based on MOF-derived porous carbon materials.

In summary, we synthesized a new nonporous NPMOF using rigid nitrogen-containing ligand and made it a porous carbon material by direct carbonization. By optimizing the pyrolysis temperatures, the material with the best performance was finally found to be NPMOF-800. The specific capacitance of NPMOF-800 can reach 220 F/g and an extremely high surface area normalized capacitance of 57.7 μF/cm^2 has been achieved, attributed to its super high heteroatom content (N: 13.91%, O: 6.27%) and ultramicroporosity features. In addition, symmetrical two-electrode device prepared by NPMOF-800 has excellent energy and power density, and the capacitance retention rate after 10,000 charge-discharge cycles is 99.1%. This work not only provides an effective way to prepare high performance supercapacitors, but also proposes new applications for numerous porous or even nonporous MOFs.

Declaration of competing interest

The authors report no declarations of interest.

Acknowledgments

This work was financially supported by the National Natural Science Foundation of China (Nos. 21501135, 21875165), the Fundamental Research Funds for the Central Universities, and the Recruitment Program of Global Experts of China.

Appendix A. Supplementary data

Supplementary material related to this article can be found, in the online version, at doi:https://doi.org/10.1016/j.cclet.2020.09.029.

References

[1] X. Chen, R. Paul, L. Dai, Natl. Sci. Rev. 4 (2017) 453–489.
[2] E. Pomerantseva, F. Bonaccorso, X. Feng, Y. Cui, Y. Gogotsi, Science 366 (2019) eaan 8285.
[3] G. Wang, L. Zhang, J. Zhang, Chem. Soc. Rev. 41 (2012) 797–828.
[4] W. Tian, H. Zhang, X. Duan, et al., Adv. Funct. Mater. 30 (2020) 1909265.
[5] H. Peng, B. Yao, X. Wei, et al., Adv. Energy Mater. 9 (2019) 1803665.
[6] R.R. Salunkhe, Y. Kamachi, N.L. Torad, et al., J. Mater. Chem. A 2 (2014) 19848–19854.
[7] H. Cheng, J. Meng, G. Wu, S. Chen, Angew. Chem. Int. Ed. 58 (2019) 17465–17473.
[8] L. Miao, Z. Song, D. Zhu, et al., Mater. Adv. 1 (2020) 945–966.
[9] J. Chmiola, G. Yushin, Y. Gogotsi, et al., Science 313 (2006) 1760–1763.
[10] N. Jäckel, P. Simon, Y. Gogotsi, V. Presser, ACS Energy Lett. 1 (2016) 1262–1265.
[11] X. Qian, L. Miao, J. Jiang, et al., Chem. Eng. J. 388 (2020) 124208.
[12] H. Jin, X. Feng, J. Li, et al., Angew. Chem. Int. Ed. 58 (2019) 2397–2401.
[13] H.F. Fei, W. Li, A. Bhardwaj, et al., J. Am. Chem. Soc. 141 (2019) 17006–17014.
[14] J. Liu, T. Yang, D.W. Wang, et al., Nat. Commun. 4 (2013) 2798.
[15] Z. Song, H. Duan, L. Miao, et al., Carbon 168 (2020) 499–507.
[16] Z. Yang, Y. Gu, B. Yuan, et al., J. Hazard. Mater. 403 (2021) 123702.
[17] G. Yuan, S. Yu, J. Jie, et al., Chin. Chem. Lett. 31 (2020) 1941.
[18] H. Furukawa, K.E. Cordova, M. O'Keeffe, O.M. Yaghi, Science 341 (2013) 1230444.
[19] Y. Tian, G. Liang, T. Fan, et al., Chem. Mater. 31 (2019) 8494–8503.
[20] S. Kitagawa, R. Kitaura, S. Noro, Angew. Chem. Int. Ed. 43 (2004) 2334–2375.
[21] L. Li, R. Matsuda, I. Tanaka, et al., J. Am. Chem. Soc. 136 (2014) 7543–7546.
[22] X. Li, X. Yang, H. Xue, H. Pang, Q. Xu, EnergyChem 2 (2020) 100027.
[23] M. Liu, F. Zhao, D. Zhu, et al., Mater. Chem. Phys. 211 (2018) 234–241.
[24] X. Li, X. Yang, H. Xue, H. Pang, Q. Xu, EnergyChem 2 (2020) 100025.
[25] B. Liu, H. Shioyama, T. Akita, Q. Xu, J. Am. Chem. Soc. 130 (2008) 5390–5391.
[26] X. Chen, D.D. Ma, B. Chen, et al., Appl. Catal. B 267 (2020) 118720.
[27] Y. Li, Y. Shan, H. Pang, Chin. Chem. Lett. 31 (2020) 2280–2286.
[28] X. Shi, S. Zhang, X. Chen, T. Tang, E. Mijowska, Carbon 157 (2020) 55–63.
[29] Q.L. Zhu, P. Pachfule, P. Strubel, et al., Energy Stor. Mater. 13 (2018) 72–79.
[30] L.D. Chen, Y.Q. Zheng, H.L. Zhu, J. Mater. Sci. 53 (2017) 1346–1355.
[31] P. Pachfule, D. Shinde, M. Majumder, Q. Xu, Nat. Chem. 8 (2016) 718–724.
[32] S. Zheng, Q. Li, H. Xue, H. Pang, Q. Xu, Natl. Sci. Rev. 7 (2020) 305–314.
[33] Y. Liu, Y. Wang, C. Shi, et al., Carbon 165 (2020) 129–138.
[34] L. Wan, E. Shamsaei, C.D. Easton, et al., Carbon 121 (2017) 330–336.
[35] Z. Li, H. Mi, L. Liu, et al., Carbon 136 (2018) 176–186.
[36] W. Chaikittisilp, M. Hu, H. Wang, et al., Chem. Commun. 48 (2012) 7159–7261.
[37] J. Yan, H. Duan, D. Zhu, et al., Electrochim. Acta 358 (2020) 136899.
[38] W. Wang, Y. Ling, L.J. Yang, et al., Res. Chem. Intermed. 42 (2015) 3157–3168.
[39] L.F. Chen, Y. Lu, L. Yu, X. Lou, Energy Environ. Sci. 10 (2017) 1777–1783.
[40] K. Jayaramulu, D.P. Dubal, B. Nagar, et al., Adv. Mater. 30 (2018) 1705789.
[41] X. Li, C. Hao, B. Tang, et al., Nanoscale 9 (2017) 2178–2187.
[42] G.W. Cong, W.Q. Peng, H.Y. Wei, et al., Appl. Phys. Lett. 88 (2006) 062110.
[43] Y. Zhang, L. Liu, L. Zhang, et al., J. Mater. Sci. 54 (2019) 6451–6460.
[44] R. Zhao, Z. Liang, S. Gao, et al., Angew. Chem. Int. Ed. 58 (2019) 1975–1979.
[45] J.X. Sun, Y.P. Yuan, L.G. Qiu, et al., Dalton Trans. 41 (2012) 6756–6763.
[46] Z. Song, L. Miao, L. Li, et al., J. Mater. Chem. A 8 (2020) 3717–3725.
[47] Z. Zhou, L. Miao, H. Duan, et al., Chin. Chem. Lett. 31 (2020) 1226–1230.
[48] M. Li, J. Xue, J. Phys. Chem. C 118 (2014) 2507–2517.
[49] F. Xu, N. Chen, Z. Fan, G. Du, Appl. Surf. Sci. 528 (2020) 146920.
[50] K. Fahsi, S.G. Dutremez, A. Vioux, L. Viau, J. Mater. Chem. A 1 (2013) 4451–5561.
[51] N.L. Torad, R.R. Salunkhe, Y. Li, et al., Chem. Eur. J. 20 (2014) 7895–7900.
[52] J. Tang, R.R. Salunkhe, J. Liu, et al., J. Am. Chem. Soc. 137 (2015) 1572–1580.
[53] P. Zhang, F. Sun, Z. Shen, D. Cao, J. Mater. Chem. A 2 (2014) 12873–12880.
[54] M. Rose, Y. Korenblit, E. Kockrick, et al., Small 7 (2011) 1108–1117.
[55] J. Zhou, M. Wang, X. Li, J. Porous Mater. 26 (2018) 99–108.
[56] H. Chen, J. Chen, D. Chen, et al., J. Mater. Sci. 54 (2018) 5625–5640.
[57] S. Zhong, C. Zhan, D. Cao, Carbon 85 (2015) 51–59.
[58] J. Hu, H. Wang, Q. Gao, H. Guo, Carbon 48 (2010) 3599–3606.
[59] L. Yao, Q. Wu, P. Zhang, et al., Adv. Mater. 30 (2018) 1706054.
[60] A. Zhang, S. Cao, Y. Zhao, C. Zhang, A. Chen, New J. Chem. 42 (2018) 6903–6909.
[61] J. Hao, J. Wang, S. Qin, et al., J. Mater. Chem. A 6 (2018) 8053–8058.
[62] Z. Hu, S. Li, P. Cheng, et al., J. Mater. Sci. 51 (2016) 2627–2633.